Measuring and Modulating Substrate Confinement during Nitrogen-Atom Transfer in a Ru_2-Based Metal-Organic Framework

Chen-Hao Wang, Wen-Yang Gao, and David C. Powers*

[1]Department of Chemistry, Texas A&M University, College Station, TX 77843, USA
*powers@chem.tamu.edu

Abstract The porosity and synthetic tunability of metal-organic frameworks (MOFs) motivate interest in application of these materials as designer heterogeneous catalysts. While *in operando* experimental evaluation of substrate mobility in these materials is critical to the rational development of highly active catalyst platforms, experimental data are rarely available. Here we demonstrate that significant substrate confinement within a microporous Ru_2-based MOF results in quantum tunneling during interstitial nitrogen-atom transfer (NAT). Further, we demonstrate that the extent of substrate confinement can be rationally tuned by modulating network mesoporosity. The reported data provide the first demonstration of tunneling during interstitial MOF chemistry and illustrate an experimental strategy to evaluate the impact of material structure on substrate mobility in porous catalysts.

Substrate confinement underpins the exquisite selectivities that characterize many enzymatic C–H oxidation reactions.[1] Substantial effort has led to the development of experimental probes to evaluate the interplay of substrate transport and substrate confinement in enzyme-catalyzed reactions. The relative magnitude of intramolecular molecular kinetic isotope effects (KIEs), obtained by challenging a catalyst with a partially labeled substrate, and intermolecular KIE, obtained by challenging a catalyst with a mixture of perlabeled and unlabeled substrate, reports on transport barriers to substrate diffusion (*i.e.* the extent of substrate commitment to participate in a

chemical step, Figure 1).[2] Further, substrate confinement within enzyme active sites often gives rise to significant quantum tunneling during C–H activation reactions (*i.e.* chemical barriers, Figure 1),[3] which manifests as large temperature-dependent intramolecular KIEs (*i.e.* $A_H/A_D < 0.7$ and $\Delta E_{D-H} > 1.2$ kcal·mol^{-1}).[4] Together, analysis of both intra- and intermolecular KIEs provides direct insight regarding *in operando* substrate mobility functionalization mechanism.

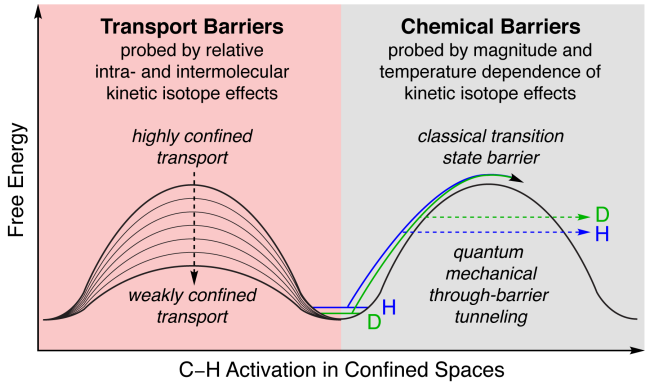

Figure 1. Comparison of intra- and intermolecular kinetic isotope effects can provide information about the degree of substrate confinement in interstitial C–H functionalization. The magnitude and temperature dependence of the kinetic isotope effect provide information about the intimate details of the C–H cleavage event.

The combination of network porosity and synthetically tunable structure has motivated interest in utilizing metal-organic frameworks (MOFs) as enzyme-mimetic catalysts.[5] Unlike enzymes, which have evolved transport mechanisms to manage substrate flux to, and product egress from, the active site, MOF catalysts rely on diffusion to manage substrate and product migration to and from lattice-confined catalyst sites.[6] Due to the inherent challenges in measuring absolute diffusivity under catalytic conditions (*i.e.* multicomponent reaction conditions) and in establishing absolute catalyst turnover frequencies in these heterogeneous systems, substrate diffusivity on timescales relevant to interstitial reaction chemistry (*i.e.* the degree of substrate confinement) is typically unknown.[7] In 2018, we reported the analysis of intra- and intermolecular KIEs to show

significant substrate confinement in the timescale of nitrogen-atom transfer (NAT) in a Ru_2-based MOF.[8] Here, we apply this experimental strategy to directly evaluate the impact of network structure on substrate mobility during interstitial chemistry. In addition to revealing systematic tuning of substrate diffusivity, the data reported here also provide the first evidence for significant quantum tunneling during C–H activation chemistry in MOFs. We anticipate that the developed experimental approach for evaluating the impact of network structure on substrate mobility will be useful in the rational design of new MOF catalysts.

We initiated our investigations by preparing a family of isostructural Ru_2-based materials with varying mesoporosities (Figure 2): Solvothermal combination of $Ru_2(OAc)_4Cl$ with mixtures of 1,3,5-benzenetricarboxylic acid (H_3btc) and 3,5-pyridinedicarboxylic acid (H_2pydc) afforded a family of materials that are isostructural to $[Ru_6(btc)_4Cl_3]$ based on powder X-ray diffraction (PXRD) analysis (Figure S1a).[9,10] Combustion analysis and surface areas (derived from 77 K N_2 adsorption isotherms; Figure S1b) of the obtained materials were consistent with previous reports of $[Ru_6(btc)_x(pydc)_{4-x}Cl_3]$ materials.[9c] Toluene vapor adsorption isotherms indicate that the gravimetric uptake of toluene is not substantially affected by introduction of mesopores and ~3 toluene molecules are adsorbed per Ru_2 site (Figure S2).[11] $[Ru_6(btc)_x(pydc)_{4-x}(N_3)_3]$ materials were accessed by soaking the corresponding chloride MOFs in DMF/H_2O solutions of NaN_3.[12] Azide-exchanged materials are isostructural to $[Ru_6(btc)_x(pydc)_{4-x}Cl_3]$ by PXRD analysis (Figure 2). Pore-size distribution analysis, based on the 77 K N_2 adsorption isotherms, provided sample-dependent mesoporous (S_{meso}) and microporous (S_{micro}) surface areas: The family of $[Ru_6(btc)_x(pydc)_{4-x}(N_3)_3]$ samples accessed in this study displayed S_{meso}/S_{micro} = 0.07–0.61 (Figure S3–S5, Table S2).[13] IR spectroscopy indicates that ν_{N3} is insensitive to network mesoporosity (ν_{N3}

= 2048 cm^{-1}), which indicates the local Ru_2N_3 structure is conserved across the family of materials (Figure S6).

We have evaluated both intra- and intermolecular KIEs for NAT to toluene to generate benzylamine as a function of network mesoporosity; the data from these experiments are summarized in Figure 3 (see Table S3 for raw data). Each k_H/k_D value was determined by thermolysis of toluene-exchanged MOF samples at 100 °C. After thermolysis, benzylamine was obtained by acidic work-up and k_H/k_D was determined by integration of high-resolution mass spectrometry.[14] Toluene amination in $[Ru_6(btc)_4(N_3)_3]$ (*i.e.* S_{meso}/S_{micro} = 0.07, "microporous" parent material) proceeds with an intramolecular k_H/k_D = 7.86(3) and an intermolecular k_H/k_D =1.02(2). These data are consistent with a scenario in which substrate self-exchange, which would mediate kinetic selection in an intermolecular competition experiment, is slow relative to NAT, and C–C rotation, which mediates kinetic selection in an intramolecular competition experiment, is faster than NAT. With increasing network mesoporosity, the intermolecular KIE, measured for NAT to a 1:1 mixture of d_8- and H_8-toluene, steadily increases from 1.02(2) to 2.33(2).[15] In contrast, the intramolecular KIE decreases from 7.86(3) for the microporous parent material to 3.4(1) for the most mesoporous sample.

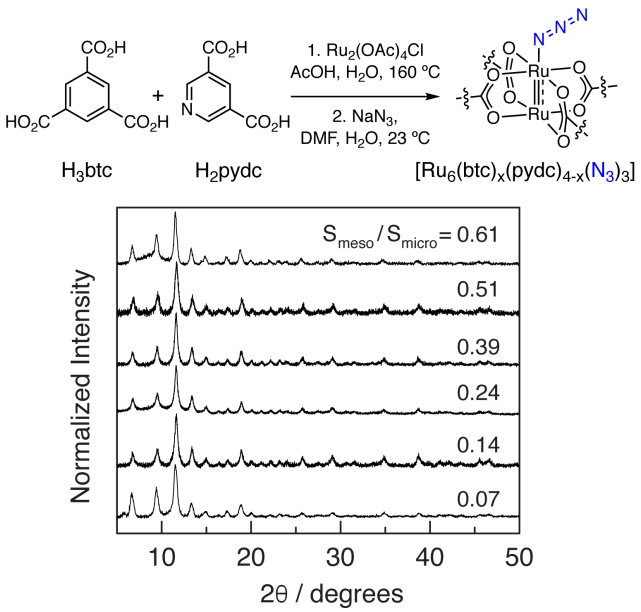

Figure 2. Synthesis of mesoporous $[Ru_6(btc)_x(pydc)_{4-x}(N_3)_3]$ via a mixed component strategy. The resulting materials are isostructural, as indicated by PXRD analysis, but display tunable mesoporosities, which are determined by fitting of the 77 K N_2 adsorption isotherms.

The data illustrated in Figure 3 provide direct experimental evidence for the impact of network mesoporosity on substrate diffusivity during interstitial functionalization chemistry. The combination of large intramolecular and negligible intramolecular KIE observed in $[Ru_6(btc)_4(N_3)_3]$ is consistent with rate-determining N_2 extrusion to generate a Ru_2 nitride,[16] and substantial substrate commitment to functionalization. These observations mirror the KIEs observed in conformationally gated enzymes[17] and in diffusionally limited zeolitic catalysts.[18] The convergence of intra- and intermolecular KIEs with increasing network mesoporosity is consistent with enhanced substrate diffusivity. Importantly, diffusion barriers are still observed in the most mesoporous samples as evidenced by the differing intra- and intermolecular KIEs (3.4 vs. 2.33).

In addition to the magnitude of kinetic isotope effects, the temperature dependence of these values can provide substantial mechanistic information regarding the intimate details of C–H cleavage. In particular, we examined the kinetic isotope effect of amination of d_1-toluene as a function of temperature (60–110 °C) with $[Ru_6(btc)_4(N_3)_3]$ ($S_{meso}/S_{micro} = 0.07$; Figure 4). We were

specifically interested in the temperature dependence of this KIE because the measured intramolecular KIE (7.86(3)) exceeds the classical limit (KIE equivalent to ~13.4 at 23 °C if treated classically). The intramolecular KIE increases substantially as the reaction temperature is decreased: amination of d_1-toluene proceeds with $k_H/k_D = 4.87$ at 110 °C, which increases to 18.8 at 60 °C (Figure 4, raw data collected in Tables S5 and S6). The reaction is prohibitively slow at lower temperatures and thus lower-temperature data are unavailable. An Arrhenius plot (Figure S8) generated from these temperature-dependent KIEs provided $A_H/A_D = 0.002$ and $\Delta E_{D-H} = 6.2 \pm 0.9$ kcal·mol^{-1} (Table 1), both of which are consistent with the criterion for tunneling articulated by Kreevoy *et al.* ($A_H/A_D < 0.7$ and $\Delta E_{D-H} > 1.2$ kcal·mol^{-1}).[4]

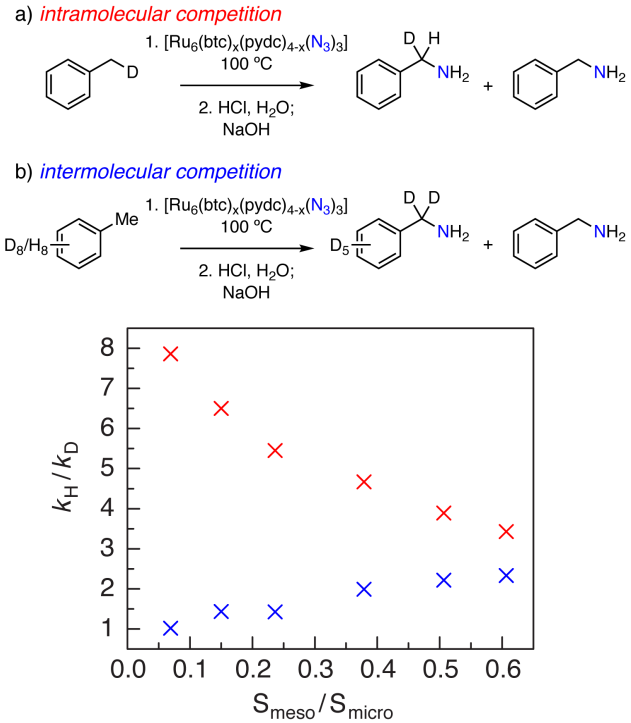

Figure 3. Plot of k_H/k_D as a function of network mesoporosity for the a) amination of d_1-toluene (×) and b) the amination of a 1:1 mixture of H_8- and d_8-toluene (×).

Further, we have analyzed the temperature dependence of the kinetic isotope effects as a function of material mesoporosity using samples with $S_{meso}/S_{micro} = 0.39$ and 0.61 (Figure 4). Amination of d_1-toluene with $S_{meso}/S_{micro} = 0.39$ [$Ru_6(btc)_x(pydc)_{4-x}(N_3)_3$] displays a temperature-

dependent KIE: from 4.67 at 110 °C to 12.1 at 60 °C. The Arrhenius plot (Figure S9) generated from these data provided $A_H/A_D = 0.007$ and $\Delta E_{D-H} = 4.9 \pm 0.9$ kcal·mol^{-1}, which is also consistent with substantial tunneling. In comparison, two temperature regimes were observed when k_H/k_D of d_1-toluene amination was determined using $S_{meso}/S_{micro} = 0.61$ [$Ru_6(btc)_x(pydc)_{4-x}(N_3)_3$] (Arrhenius plot presented in Figure S10). Between 90–110 °C, the observed NAT displays classical Arrhenius behavior ($A_H/A_D = 0.87$ and $\Delta E_{D-H} = 1.0 \pm 0.3$ kcal·mol^{-1}). Below 90 °C, temperature dependent KIEs are observed and Arrhenius analysis suggests the contribution of tunneling ($A_H/A_D = 0.001$ and $\Delta E_{D-H} = 6.1 \pm 1.2$ kcal·mol^{-1}). These observations indicate that toluene confinement in the most mesoporous sample is relaxed such that NAT displays classical kinetic behavior at high temperature.

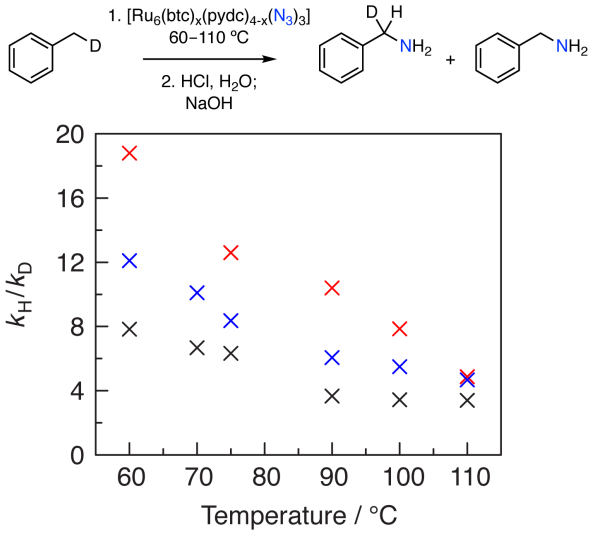

Figure 4. Temperature-dependent intramolecular KIEs for the amination of d_1-toluene in [$Ru_6(btc)_4(N_3)_3$] (×, $S_{meso}/S_{micro} = 0.07$) and [$Ru_6(btc)_x(pydc)_{4-x}(N_3)_3$] with $S_{meso}/S_{micro} = 0.39$ (×) and 0.61 (×).

Table 1. Arrhenius parameters for C–H amination derived from temperature-dependent KIEs.

S_{meso} / S_{micro}	A_H/A_D	ΔE_{D-H} (kcal·mol^{-1})	R^2
0.07	0.002	6.2 ± 0.9	0.94
0.39	0.007	4.9 ± 0.3	0.98
0.61 (>90 °C)	0.87	1.0 ± 0.3	0.84
0.61 (<90 °C)	0.001	6.1 ± 1.2	0.93

The combination of large KIE values and the observed temperature dependences suggests that tunneling contributes meaningfully to the rate of HAA during NAT at lattice-confined Ru_2 nitrides. By manipulating the mesoporosity of the material we have accessed a set of conditions in which NAT chemistry behaves classically. These results closely mirror those reported by Klinman *et al.* for H-atom abstraction (HAA) reactions mediated by I553X series of soybean lipoxygenase (SLO) variants which showed the tunneling effect was less substantial as pre-tunneling distance was increased.[19]

Further support for substantial substrate confinement and the contribution of tunneling to HAA chemistry mediated by lattice-confined Ru_2 nitride intermediates was obtained by examination of the amination of selectively labeled xylenes featuring one CH_3 and one CD_3 group. Labeled xylene isomers were prepared by Suzuki coupling between the appropriate tolylboronic acid and d_3-methyl iodide.[20] Using a sample of $[Ru_6(btc)_x(pydc)_{4-x}(N_3)_3]$ with S_{meso}/S_{micro} = 0.61 we have carried out amination of each of the labeled xylene isomers (Table 2). Each isomer participates in amination upon thermolysis at 100 °C to afford the corresponding methylbenzylamine and displays large kinetic isotope effect (k_H/k_D = 29.3 (*ortho*-xylene), 26.0 (*meta*), and 25.8 (*para*). The similarity of these KIE values indicates that the methyl groups of each isomer are exchanging on the timescale of NAT; if xylene was sufficiently confined to prevent exchange of the methyl groups one would expect *p*-d_3-xylene would display a much lower KIE than *o*-d_3-xylene. Each of the measured KIEs is highly temperature dependent: When thermolysis is carried out at 130 °C, k_H/k_D values of 15.4 (*ortho*), 11.9 (*meta*), and 12.8 (*para*) are obtained. The enhanced KIE values for xylene amination as compared to toluene suggest that xylenes (kinetic diameter (7.4 Å (*ortho*), 7.1 Å (*meta*), and 6.7 Å (*para*),[21] are more confined in a given network than toluene (kinetic diameter (5.9 Å)).[22]

Table 1. Temperature-dependent KIEs for NAT to isomeric d_3-xylenes using $[Ru_6(btc)_x(pydc)_{4-x}(N_3)_3]$ (S_{meso} / S_{micro} = 0.61).

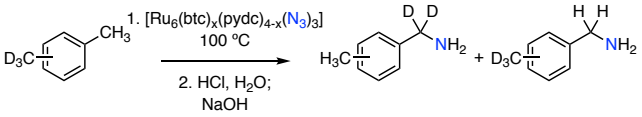

Substrate	k_H/k_D			
	100 °C	110 °C	120 °C	130 °C
o-d_3-xylene	29.3	27.7	15.8	15.4
m-d_3-xylene	26.0	22.1	19.9	11.9
p-d_3-xylene	25.8	20.4	14.5	12.8

In conclusion, the described experimental results directly reveal the impact of network structure on the confinement of substrates during interstitial chemistry. Because the experiments provide *in operando* observation of the relative rates of substrate diffusion and functionalization, this analysis is amenable to application in the commonly encountered defective frameworks that are utilized in MOF catalysis. In addition, these experiments have revealed that network-dependent substrate confinement gives rise to substantial quantum tunneling during interstitial C–H functionalization chemistry. These data highlight the similarity of pore-confined substrate functionalization with enzymatic C–H functionalization and serve as a stark example of the significant transport barriers that confront fine-chemical synthesis in microporous MOFs. We anticipate the described experiments will provide critical *in operando* information regarding diffusivity that will inform rational development of designer MOF catalysts.

Acknowledgement

This research was supported by the U.S. Department of Energy, Office of Science, Office of Basic Energy Sciences, Catalysis program, under award DE-SC-0001234. The authors additionally

thank The Welch Foundation (A-1907) for supporting preliminary experimental work. We thank Eric Bloch for toluene vapor adsorption data.

References

(1) (a) Benkovic, S. J.; Hammes-Schiffer, S. A Perspective on Enzyme Catalysis. *Science* **2003**, *301*, 1196–1202. (b) Ortiz de Montellano, P. R. Hydrocarbon Hydroxylation by Cytochrome P450 Enzymes. *Chem. Rev.* **2010**, *110*, 932–948. (c) Huang, X.; Groves, J. T. Oxygen Activation and Radical Transformations in Heme Proteins and Metalloporphyrins. *Chem. Rev.* **2018**, *118*, 2491–2553.

(2) Northrop, D. B. Deuterium and Tritium Kinetic Isotope Effects. *Methods Enzymol.* **1982**, *87*, 607–625.

(3) Klinman, J. P.; Offenbacher, A. R. Understanding Biological Hydrogen Transfer through the Lens of Temperature Dependent Kinetic Isotope Effects. *Acc. Chem. Res.* **2018**, *51*, 1966–1974.

(4) Kim, Y.; Kreevoy, M. M. The Experimental Manifestations of Corner-Cutting Tunneling. *J. Am. Chem. Soc.* **1992**, *114*, 7116–7123.

(5) (a) Lee, J.; Farha, O. K.; Roberts, J.; Scheidt, K. A.; Nguyen, S. T.; Hupp, J. T. Metal-organic framework materials as catalysts. *Chem. Soc. Rev.* **2009**, *38*, 1450–1459. (b) Gu, Z.-Y.; Park, J.; Raiff, A.; Wei, Z.; Zhou, H.-C. Metal-Organic Frameworks as Biomimetic Catalysts. *ChemCatChem* **2014**, *6*, 67–75. (c) Nath, I.; Chakraborty, J.; Verpoort, F. Metal organic frameworks mimicking natural enzymes: a structural and functional analogy. *Chem. Soc. Rev.* **2016**, *45*, 4127–4170. (d) Rogge, S. M. J.; Bavykina, A.; Hajek, J.; Garcia, H.; Olivos-Suarez, A. I.; Sepúlveda-Escribano, A.; Vimont, A.; Clet, G.; Bazin, P.; Kapteijn, F.; Daturi, M.; Ramos-Fernandez, E. V.; Llabrés i Xamena, F. X.; Speybroeck, V. V.; Gascon, J. Metal-organic and covalent organic frameworks as single-site catalysts. *Chem. Soc. Rev.* **2017**, *46*, 3134–3184.

(6) Krishna, R. Diffusion in porous crystalline materials. *Chem. Soc. Rev.* **2012**, *41*, 3099–3118.

(7) (a) Yang, D.; Gates, B. C. Catalysis by Metal Organic Frameworks: Perspective and Suggestion for Future Research. *ACS Catal.* **2019**, *9*, 1779–1798. (b) Pascanu, V.; Miera, G. G.; Inge, A. K.; Martín-Matute, B. Metal-Organic Frameworks as Catalysts for Organic Synthesis: A Critical Perspective. **2019**, *141*, 7223–7234.

(8) Wang, C.-H.; Das, A.; Gao, W.-Y.; Powers, D. C. Probing Substrate Diffusion in Interstitial MOF Chemistry with Kinetic Isotope Effects. *Angew. Chem., Int. Ed.* **2018**, *57*, 3676–3681.

(9) (a) Marx, S.; Kleist, W.; Baiker, A. Synthesis, structural properties, and catalytic behavior of Cu-BTC and mixed-linker Cu-BTC-PyDC in the oxidation of benzene derivatives. *J. Catal.* **2011**, *281*, 76–87. (b) Fang, Z.; Dürholt, J. P.; Kauer, M.; Zhang, W.; Lochenie, C.; Jee, B.; Albada, B.; Metzler-Nolte, N.; Pöppl, A.; Weber, B.; Muhler, M.; Wang, Y.; Schmid, R.; Fischer, R. A. Structural Complexity in Metal–Organic Frameworks: Simultaneous Modification of Open Metal Sites and Hierarchical Porosity by Systematic Doping with Defective Linkers. *J. Am. Chem. Soc.* **2014**, *136*, 9627–9636. (c)Kozachuk, O.; Luz, I.; Llabrés I Xamena, F. X.; Noei, H.; Kauer, M.; Albada, H. B.; Bloch, E. D.; Marler, B.; Wang, Y.; Muhler, M.; Fischer, R. A. Multifunctional, Defect-Engineered Metal–Organic Frameworks with Ruthenium Centers: Sorption and Catalytic Properties. *Angew. Chem., Int. Ed.* **2014**, *53*, 7058–7062.

(10) Isoreticular Ru_2-based materials are not available and extensive synthetic efforts have not provided access to pore-expanded structures.

(11) Li, Y.; Miao, J.; Sun, X.; Xiao, J.; Li, Y.; Wang, H.; Xia, Q.; Li, Z. Mechanochemical synthesis of Cu-BTC@GO with enhanced water stability and toluene adsorption capacity. *Chem. Eng. J.* **2016**, *298*, 191–197.

(12) For analysis of the ligand occupancy in the apical position of Ru_2 sites, see Supporting Information.

(13) Samples with higher mesoporosities are unavailable; attempts to access such samples resulted in decreased crystallinity.

(14) The isotopic composition of the obtained benzylamine is insensitive to the acid employed during work-up (*i.e.* DCl *vs.* HCl).

(15) The observed intermolecular KIEs are independent of reaction progress, confirming these values arise from kinetic selection (Table S4).

(16) Consistent with the lack of participation of C–H bonds in the rate determining step, the disappearance of the azide signal in the IR proceeds at identical rates for completely activated samples and for toluene impregnated samples (Figure S7).

(17) In the context of methane monooxygenase activity, see: Priestley, N. D.; Floss, H. G.; Froland, W. A.; Lipscomb, J. D.; Williams, P. G.; Morimoto, H. Cryptic Stereospecificity of Methane Monooxygenase. *J. Am. Chem. Soc.* **1992**, *114*, 7561–7562 (intramolecular KIEs). Brazeau, B. J.; Wallar, B. J.; Lipscomb, J. D.

Unmasking of Deuterium Kinetic Isoptope Effects on the Methane Monooxygenase Compound Q Reaction by Site-Directed Mutagenesis of Component B. *J. Am. Chem. Soc.* **2001**, *123*, 10421–10422 (intermolecular KIEs).

(18) Dubkov, K. A.; Sobolev, V. I.; Talsi, E. P.; Rodkin, M. A.; Watkins, N. H.; Shteinman, A. A.; Panov, G. I. Kinetic isotope effects and mechanism of biomimetic oxidation of methane and benzene on FeZSM-5 zeolite. *J. Mol. Cat. A* **1997**, *123*, 155–161.

(19) Jonsson, T.; Glickman, M. H.; Sun, S.; Klinman, J. P. Experimental Evidence for Extensive Tunneling of Hydrogen in the Lipoxygenase Reaction: Implications for Enzyme Catalysis. *J. Am. Chem. Soc.* **1996,** *118*, 10319–10320.

(20) Gooßen, L. J. A simple and practical protocol for the palladium-catalyzed cross-coupling of boronic acids with methyl iodide. *Appl. Organometal. Chem.* **2004**, *18*, 602–604.

(21) Peralta, D.; Barthelet, K.; Perez-Pellitero, J.; Chizallet, C.; Chaplais, G.; Simon-Masseron, A.; Pirngruber, G. D. Adsorption and Separation of Xylene Isomers: CPO-27-Ni vs HKUST-1 vs NaY. *J. Phys. Chem. C* **2012**, *116*, 21844−21855.

(22) Goel, S.; Wu, Z.; Zones, S. I.; Iglesia, E. Synthesis and Catalytic Properties of Metal Clusters Encapsulated within Small-Pore (SOD, GIS, ANA) Zeolites. *J. Am. Chem. Soc.* **2012**, *134*, 17688−17695.